Annals of Nuclear Energy 216 (2025) 111250

Contents lists available at ScienceDirect

Annals of Nuclear Energy

journal homepage: www.elsevier.com/locate/anucene

A nonclassical model to eigenvalue neutron transport calculations

Leonardo R.C. Moraes [a,*], Ricardo C. Barros [a], Hermes Alves Filho [a], Richard Vasques [b]

[a] Universidade do Estado do Rio de Janeiro, Programa de Pós-graduação em Modelagem Computacional – IPRJ, Rua Bonfim 25, 28625-570, Nova Friburgo, RJ, Brazil

[b] The Ohio State University, Department of Mechanical and Aerospace Engineering, 201 W. 19th Avenue, Columbus, OH 43210, United States of America

ARTICLE INFO

Keywords:
Nonclassical transport
Eigenvalue calculations
Spectral approach
Random media
Slab geometry

ABSTRACT

In this work, we present an extension of the nonclassical transport model, namely the generalized linear Boltzmann equation (GLBE), to eigenvalue criticality problems. The GLBE is a generalization of the linear Boltzmann equation that allows the modeling of particle transport in random statistically homogeneous systems in which the free-path distribution function $p(\boldsymbol{\Omega}, s)$ is non-exponential. This type of problem is referred to as a nonclassical transport problem. The model's ability to accurately replicate the expected value for the system's effective multiplication factor and the profile of the neutron scalar flux for both classical and nonclassical transport problems is analyzed.

1. Introduction

Stochastic transport problems form a class of particle transport problems where the material parameters are known only in a statistical sense. The generation of the expected particle intensity in phase space is usually the primary objective in problems of this nature. The most common technique used for calculating the expected particle intensity is the direct method (Adams et al., 1989; Olson, 2007; Pomraning, 2002; Su and Pomraning, 1993). In this method, the conventional linear transport equation (Prinja and Larsen, 2010) is solved for a variety of possible physical configurations, and the average of these solutions is used as the expected particle intensity. Although fairly simple to implement, the direct method needs to take into account a large number of physical configurations to produce an average solution with a small variance, which is why it is frequently avoided.

The potential challenges that the direct method may impose concerning time efficiency have pushed forward the development of a number of methods to solve stochastic problems. In the most notable method developed, namely the Atomic Mix method (Torquato et al., 2000; Dumas and Golse, 2000; Pomraning, 1991), the expected particle intensity is obtained through the solution of the linear transport equation considering volume-averaged homogenized cross sections. Nonetheless, there are some stochastic problems where the Atomic Mix method cannot yield reliable results. Contrary to the exponential attenuation (linear transport model) assumed in the Atomic Mix method, correlations between scattering centers and/or unresolved spatial fluctuations in the system cause the flux of particles in these problems to decay non-exponentially (Larsen and Vasques, 2011; Vasques and Larsen, 2009; Davis and Marshak, 2004; Davis, 2004; Davis and Xu, 2014; Davis and Mineev-Weinstein, 2009). This group of stochastic problems, namely nonclassical problems, is the focus of the nonclassical particle transport theory.

The generalized linear transport equation (GLBE) is a mathematical model that can be used to simulate fixed-source nonclassical particle transport problems. It was first derived by Larsen in Larsen (2007) to describe measurements of photon path-length in the Earth's cloudy atmosphere that could not be explained by classical radiative transfer. Although first used in the radiative transfer context, the nonclassical transport model found its way into a variety of areas such as computer graphics (Jarabo et al., 2018; Bitterli et al., 2018; Wrenninge et al., 2017), and reactor physics (Vasques and Larsen, 2009, 2014c; Vasques, 2013; Vasques et al., 2017). Moreover, the development of methods to efficiently solve the GLBE is nowadays an active area of research (Patel et al., 2022; Moraes et al., 2022c,a, 2023b; Vasques et al., 2020).

Differently from fixed-source particle transport problems, where the goal is, given the incidence of particles through the boundaries and/or interior particle sources, to calculate the particle intensity in the system (or the expected particle intensity in stochastic problems), in the so-called eigenvalue particle transport problems, the main goal is to estimate the effective multiplication factor (k_{eff}) of the system. In nuclear reactor physics, k_{eff} expresses the ratio of the neutrons produced by fission in one generation to the number of neutrons lost through absorption and leakage in the preceding generation within the

* Corresponding author.
E-mail addresses: lrcmoraes@iprj.uerj.br (L.R.C. Moraes), ricardob@iprj.uerj.br (R.C. Barros), halves@iprj.uerj.br (H.A. Filho), vasques.4@osu.edu (R. Vasques).

https://doi.org/10.1016/j.anucene.2025.111250
Received 30 September 2024; Received in revised form 23 December 2024; Accepted 4 February 2025

system. The accurate calculation of this quantity is important since it indicates whether the chain fission reaction in the system can be sustained. The k_{eff} is of particular interest in the design of nuclear reactors and in the safety analysis of a reactor (Romojaro et al., 2017; Li-Po et al., 2008; Gandini and Salvatores, 2002; Moraes et al., 2022b, 2021).

In this work, we extend the nonclassical particle transport model (Vasques and Larsen, 2014a) to eigenvalue calculations. This extension is motivated by the concept of the Gen IV Pebble Bed Reactors (PBR) (Kadak, 2005; Gougar et al., 2010; Lohnert and Reutler, 1983; Moormann, 2009; Ge et al., 2016). The basic design of PBR features a reactor core composed of a bed of spherical fuel elements (pebbles) consisting of thousands of fuel particles embedded in a graphite matrix. Hundreds of thousands are randomly packed in the reactor core generating a sustained fission chain reaction which is cooled by high-pressure gas forced through the interstitial spaces between the pebbles. Due to this dynamic structuring, the exact locations of the pebbles inside the core at any given time are unknown (stochastic problem). Moreover, the fact that pebbles are O(1) mean free paths thick calls into question the validity of the atomic mix approximation (Larsen et al., 2005). That stimulates the development of different methodologies to calculate the effective multiplication factor in nonclassical systems, such as the one presented in this paper. At this point, we remark that although our motivation resides on the concept of the PBR, we are not tackling PBR problems in this work. Our focus is to derive a mathematical model to eigenvalue calculations that can be applied to different nonclassical problems in fission-chain reacting systems.

A summary of the remainder of this paper is given next. In Section 2 we present the derivation of a particle transport equation for nonclassical eigenvalue problems (k_{eff}-GLBE). In Section 3 we briefly describe a solution process for the one-dimensional version of the k_{eff}-GLBE in the discrete ordinates (S_N) formulation. We have chosen to deal with the one-dimensional version of the k_{eff}-GLBE since, to our knowledge, this is the first attempt to use the nonclassical transport model in eigenvalue calculations. Numerical results are given in Section 4 to analyze the model's ability to accurately replicate the expected value for the system's effective multiplication factor and the profile of the neutron scalar flux for both classical and nonclassical transport problems. We finish with a number of concluding remarks in Section 5.

2. A nonclassical particle transport equation for eigenvalue calculations

Differently from classical problems, in nonclassical transport problems the incremental probability dp that a particle will collide while traveling an incremental distance ds is considered as (Vasques and Larsen, 2014a)

$$dp = \Sigma_t(\boldsymbol{x}, \boldsymbol{\Omega}, s)ds, \tag{2.1}$$

where $\boldsymbol{x} = (x, y, z)$ is a point of space, $\boldsymbol{\Omega} = (\Omega_x, \Omega_y, \Omega_z)$ is the particle's direction of flight, such that $|\boldsymbol{\Omega}| = 1$, s is the path-length, i.e., the distance traveled by the particle since its last interaction (birth or scattering), and Σ_t is the total macroscopic cross-section. The components of $\boldsymbol{\Omega}$ are $\Omega_x = \sqrt{1-\mu^2}\,cos\phi$, $\Omega_y = \sqrt{1-\mu^2}\,sin\phi$ and $\Omega_z = \mu$, where $\mu = cos\theta$ and $d\Omega = d\mu d\phi$ with θ and ϕ being the polar and azimuthal angles respectively. We remark that in more general problems Σ_t will also be dependent of the particle's kinetic energy.

As we can see in Eq. (2.1), in nonclassical transport problems the total cross section is dependent not only of $\boldsymbol{x}$ (as in classical problems) but also of $\boldsymbol{\Omega}$ and s. The idea of making Σ_t also dependent of $\boldsymbol{\Omega}$ and s is that by extending the phase-space of Σ_t we make it possible to mathematically model transport problems where the particle flux is not necessarily exponentially attenuated. To visualize this modeling extension, let us consider, with no loss of generality, a homogenized system (Σ_t is not dependent of $\boldsymbol{x}$). Moreover, we define $N(\boldsymbol{\Omega}, s)$ as the number of particles that have traveled a distance s in the direction $\boldsymbol{\Omega}$ without experiencing collisions. Using a similar definition, $N(\boldsymbol{\Omega}, s+ds)$ is the number of particles that have traveled a distance $s + ds$ in $\boldsymbol{\Omega}$ without experiencing collisions. The quantity $N(\boldsymbol{\Omega}, s + ds)$ can be rewritten as a truncated Taylor Series (Anon, 2008) as

$$N(\boldsymbol{\Omega}, s + ds) = N(\boldsymbol{\Omega}, s) + \frac{\partial}{\partial s}N(\boldsymbol{\Omega}, s)ds. \tag{2.2}$$

Rearranging the terms of Eq. (2.2), and dividing the resulting equation by $N(\boldsymbol{\Omega}, s)$ we obtain the following expression

$$-\frac{N(\boldsymbol{\Omega}, s) - N(\boldsymbol{\Omega}, s + ds)}{N(\boldsymbol{\Omega}, s)} = \frac{1}{N(\boldsymbol{\Omega}, s)}\frac{\partial}{\partial s}N(\boldsymbol{\Omega}, s)ds. \tag{2.3}$$

If we pay close attention to Eq. (2.3), we notice that the left-hand side of this equation is equal to the probability that a particle migrating in $\boldsymbol{\Omega}$ will have a collision while traveling an incremental distance ds in the system. That is,

$$-\Sigma_t(\boldsymbol{\Omega}, s)ds = \frac{1}{N(\boldsymbol{\Omega}, s)}\frac{\partial}{\partial s}N(\boldsymbol{\Omega}, s)ds, \tag{2.4a}$$

which is equivalent to

$$\frac{\partial}{\partial s}N(\boldsymbol{\Omega}, s) + \Sigma_t(\boldsymbol{\Omega}, s)N(\boldsymbol{\Omega}, s) = 0. \tag{2.4b}$$

The solution of Eq. (2.4b) takes the form

$$N(\boldsymbol{\Omega}, s) = N_0(\boldsymbol{\Omega})e^{-\int_0^s \Sigma_t(\boldsymbol{\Omega}, s')ds'}, \tag{2.5}$$

where $N_0(\boldsymbol{\Omega}) = N(0, \boldsymbol{\Omega})$ is the initial ($s = 0$) number of neutrons migrating in the direction of $\boldsymbol{\Omega}$. If classical transport takes place then $\Sigma_t(\boldsymbol{\Omega}, s) = \Sigma_t$, and Eq. (2.5) becomes

$$N(\boldsymbol{\Omega}, s) = N_0(\boldsymbol{\Omega})e^{-\Sigma_t s}. \tag{2.6}$$

From Eq. (2.6) we notice that by considering the total cross section as independent of $\boldsymbol{\Omega}$ and s, we are inherently assuming that the particle flux is exponentially attenuated. On the other hand, the consideration of Σ_t as a function of $\boldsymbol{\Omega}$ and s allows the mathematical modeling of transport problems where the particle flux is not exponentially attenuated. According to Eq. (2.5), the particle flux can assume characteristics other than exponential, depending on the choice of $\Sigma_t(\boldsymbol{\Omega}, s)$. Following the phase-space extension of Σ_t, a particle transport equation for nonclassical eigenvalue calculations is derived next.

2.1. Derivation of the k_{eff} GLBE

We begin by imposing some assumptions about the problem and introducing some definitions that are going to be used in the derivation of the k_{eff} GLBE:

- The system is infinite and statistically homogeneous;
- The particle considered is the neutron, and the transport is monoenergetic;
- $\Sigma_t(\boldsymbol{x}, \boldsymbol{\Omega}, s) = \Sigma_t(\boldsymbol{\Omega}, s)$ is a known function. As the material parameters are known only in a statistical sense in nonclassical problems, the true cross-section of the problem $\Sigma_t(\boldsymbol{x}, \boldsymbol{\Omega}, s)$ is replaced by the homogenized cross-section $\Sigma_t(\boldsymbol{\Omega}, s)$. The generation of accurate cross sections $\Sigma_t(\boldsymbol{\Omega}, s)$ is crucial, and can be a challenging task. Reference Larsen and Vasques (2011) provide details about this calculation;
- The phase space that represents the system is extended to include the variable s. Moreover, $n(\boldsymbol{x}, \boldsymbol{\Omega}, s)$ represents the neutron angular density, and $N(\boldsymbol{x}, \boldsymbol{\Omega}, s) = n(\boldsymbol{x}, \boldsymbol{\Omega}, s)dVd\Omega ds$ is the number of neutrons in $dVd\Omega ds$ about $(\boldsymbol{x}, \boldsymbol{\Omega}, s)$ at time t;
- The neutron speed is $v = \frac{ds}{dt}$, and the angular flux density is $\Psi(\boldsymbol{x}, \boldsymbol{\Omega}, s) = vn(\boldsymbol{x}, \boldsymbol{\Omega}, s)$. Moreover, $\Psi \to 0$ when $|\boldsymbol{x}| \to \infty$ and/or $s \to \infty$;
- c_s and c_f are, respectively, the probabilities that a neutron when collides will scatter or induce fission. These constants are not functions of either $\boldsymbol{\Omega}$ and s since these variables affect only the collision probability of a neutron. Thus, c_s and c_f are probabilities associated with neutrons that already have experienced a collision;

- $P(\boldsymbol{\Omega}' \cdot \boldsymbol{\Omega})d\Omega$ is the probability that when a neutron migrating in the direction $\boldsymbol{\Omega}'$ scatters it will migrate in $d\Omega$ about $\boldsymbol{\Omega}$. This quantity is independent of s since it presumes that the neutron already has experienced a collision;
- All neutrons released in fission events are considered "prompt", i.e., they are instantly released after fission reactions. In addition, ν represents the average number of neutrons released in a fission event.

A particle transport equation is a conservation equation, i.e, it mathematically represents the balance between gain and losses of a certain type of particle in the system. In the case of this work, this balance is represented as

$$\{\text{Rate of change} = \text{Rate of gain} - \text{Rate of loss}\} \text{ of neutrons in } dVd\Omega ds \text{ about } (\boldsymbol{x}, \boldsymbol{\Omega}, s). \tag{2.7}$$

The rate of change of neutrons can be obtained by taking the derivative of the angular flux with respect to the variable s. That is,

$$\begin{aligned}&\text{Rate of change of neutrons in } dVd\Omega ds \text{ about } (\boldsymbol{x}, \boldsymbol{\Omega}, s)\\ &= \frac{\partial}{\partial s}\Psi(\boldsymbol{x}, \boldsymbol{\Omega}, s)dVd\Omega ds\\ &= \frac{\partial}{\partial s}\frac{ds}{dt}n(\boldsymbol{x}, \boldsymbol{\Omega}, s)dVd\Omega ds\\ &= \frac{\partial}{\partial t}n(\boldsymbol{x}, \boldsymbol{\Omega}, s)dVd\Omega ds.\end{aligned} \tag{2.8}$$

Now, concerning the rate of losses, two events are responsible for the loss of neutrons: (I) the collision of neutrons with the nucleons that compose the background materials; and (II) the migration of neutrons out of the system. The collision rate term can be written as

$$\begin{aligned}\Sigma_t(\boldsymbol{\Omega}, s)\Psi(\boldsymbol{x}, \boldsymbol{\Omega}, s)dVd\Omega ds &= \Sigma_t(\boldsymbol{\Omega}, s)\frac{ds}{dt}n(\boldsymbol{x}, \boldsymbol{\Omega}, s)dVd\Omega ds\\ &= \frac{1}{dt}\left[\Sigma_t(\boldsymbol{\Omega}, s)ds\right]n(\boldsymbol{x}, \boldsymbol{\Omega}, s)dVd\Omega ds\\ &= \text{rate at which neutrons in } dVd\Omega ds \text{ about}\\ &\quad (\boldsymbol{x}, \boldsymbol{\Omega}, s)\\ &\quad \text{experience collisions.}\end{aligned} \tag{2.9}$$

The migration term represents the net rate at which neutrons will leak out the system. This is represented as

$$\begin{aligned}|\boldsymbol{\Omega}\cdot\boldsymbol{n}|\Psi(\boldsymbol{x}, \boldsymbol{\Omega}, s)dSd\Omega ds = &\text{ rate at which neutrons in } d\Omega ds \text{ about } (\boldsymbol{\Omega}, s)\\ &\text{flow through the incremental surface } dS\\ &\text{with unit outward normal vector } \boldsymbol{n}.\end{aligned} \tag{2.10a}$$

Making use of the divergence theorem (Stewart, 2009), we rewrite Eq. (2.10a) as

$$\begin{aligned}\boldsymbol{\Omega}\cdot\nabla\Psi(\boldsymbol{x}, \boldsymbol{\Omega}, s)dVd\Omega ds = &\text{ net rate of neutrons in } d\Omega ds \text{ about } (\boldsymbol{\Omega}, s)\\ &\text{that leak out } dV \text{ about } \boldsymbol{x}.\end{aligned} \tag{2.10b}$$

Using Eqs. (2.9) and (2.10b) we define the rate of loss as

$$\begin{aligned}&\text{Rate of loss of neutrons in } dVd\Omega ds \text{ about } (\boldsymbol{x}, \boldsymbol{\Omega}, s) =\\ &\left[\Sigma_t(\boldsymbol{\Omega}, s)\Psi(\boldsymbol{x}, \boldsymbol{\Omega}, s) + \boldsymbol{\Omega}\cdot\nabla\Psi(\boldsymbol{x}, \boldsymbol{\Omega}, s)\right]dVd\Omega ds.\end{aligned} \tag{2.11}$$

Once the rate of loss is defined, we focus our attention on the rate of gain. In multiplying systems, various reactions can contribute to neutron gain. However, only two reactions, namely in-scatter and fission reactions, will be considered in this derivation. The reason is that their occurrence rate is much larger compared to other reactions that promote neutron gain. Therefore, reactions other than in-scatter and fission can be neglected without loss of precision. To describe the rates of gain associated with in-scatter and fission reactions we first define

$$\begin{aligned}&\left[\int_0^\infty \Sigma_t(\boldsymbol{\Omega}', s')\Psi(\boldsymbol{x}, \boldsymbol{\Omega}', s')ds'\right]dVd\Omega'\\ &= \text{rate at which neutrons in } dVd\Omega'\\ &\quad \text{about } (\boldsymbol{x}, \boldsymbol{\Omega}') \text{ experience collisions.}\end{aligned} \tag{2.12}$$

Multiplying Eq. (2.12) by $\frac{\nu c_f}{4\pi}d\Omega$ and integrating the resulting equation over $\Omega' \in 4\pi$ we obtain

$$\begin{aligned}&\left[\int_{4\pi}\int_0^\infty \frac{\nu c_f}{4\pi}\Sigma_t(\boldsymbol{\Omega}', s')\Psi(\boldsymbol{x}, \boldsymbol{\Omega}', s')ds'd\Omega'\right]dVd\Omega\\ &= \text{rate at which neutrons are released}\\ &\text{in } dVd\Omega \text{ about } (\boldsymbol{x}, \boldsymbol{\Omega}) \text{ from fission reactions.}\end{aligned} \tag{2.13a}$$

Following a similar procedure, we multiply Eq. (2.12) by $c_s P(\boldsymbol{\Omega}'\cdot\boldsymbol{\Omega})d\Omega$ and integrate the resulting equation over $\Omega' \in 4\pi$, thus obtaining

$$\begin{aligned}&\left[\int_{4\pi}\int_0^\infty c_s P(\boldsymbol{\Omega}'\cdot\boldsymbol{\Omega})\Sigma_t(\boldsymbol{\Omega}', s')\Psi(\boldsymbol{x}, \boldsymbol{\Omega}', s')ds'd\Omega'\right]dVd\Omega\\ &= \text{rate at which neutrons}\\ &\text{scatter into } dVd\Omega \text{ about } (\boldsymbol{x}, \boldsymbol{\Omega}).\end{aligned} \tag{2.13b}$$

At this point, we recall the definition of the variable s, i.e., the distance traveled by the particle since its last interaction. This means that neutrons released in fission and scattering reactions have their s variable set to zero. Therefore, the path-length spectrum of neutrons that emerge from these reactions is the delta function $\delta(s)$. Thus, multiplying Eqs. (2.13) by $\delta(s)ds$ we obtain

$$\begin{aligned}&\left[\delta(s)\int_{4\pi}\int_0^\infty \frac{\nu c_f}{4\pi}\Sigma_t(\boldsymbol{\Omega}', s')\Psi(\boldsymbol{x}, \boldsymbol{\Omega}', s')ds'd\Omega'\right]dVd\Omega ds\\ &= \text{rate at which neutrons are released}\\ &\text{in } dVd\Omega\text{ds about } (\boldsymbol{x}, \boldsymbol{\Omega}, s) \text{ from fission reactions}\end{aligned} \tag{2.14a}$$

and

$$\begin{aligned}&\left[\delta(s)\int_{4\pi}\int_0^\infty c_s P(\boldsymbol{\Omega}'\cdot\boldsymbol{\Omega})\Sigma_t(\boldsymbol{\Omega}', s')\Psi(\boldsymbol{x}, \boldsymbol{\Omega}', s')ds'd\Omega'\right]dVd\Omega ds\\ &= \text{rate at which neutrons}\\ &\text{scatter into } dVd\Omega ds \text{ about } (\boldsymbol{x}, \boldsymbol{\Omega}, s).\end{aligned} \tag{2.14b}$$

Summing Eqs. (2.14), we obtain the rate of gain, i.e.,

$$\begin{aligned}&\text{Rate of gain of neutrons in } dVd\Omega ds \text{ about } (\boldsymbol{x}, \boldsymbol{\Omega}, s) =\\ &\delta(s)\left[\int_{4\pi}\int_0^\infty \frac{\nu c_f}{4\pi}\Sigma_t(\boldsymbol{\Omega}', s')\Psi(\boldsymbol{x}, \boldsymbol{\Omega}', s')ds'd\Omega'\right.\\ &\left.+\int_{4\pi}\int_0^\infty c_s P(\boldsymbol{\Omega}'\cdot\boldsymbol{\Omega})\Sigma_t(\boldsymbol{\Omega}', s')\Psi(\boldsymbol{x}, \boldsymbol{\Omega}', s')ds'd\Omega'\right]dVd\Omega ds.\end{aligned} \tag{2.15}$$

Substituting Eqs. (2.11) and (2.15) into Eq. (2.7), and dividing the resulting equation by $dVd\Omega ds$ we obtain

$$\begin{aligned}&\frac{\partial}{\partial s}\Psi(\boldsymbol{x}, \boldsymbol{\Omega}, s) + \Sigma_t(\boldsymbol{\Omega}, s)\Psi(\boldsymbol{x}, \boldsymbol{\Omega}, s) + \boldsymbol{\Omega}\cdot\nabla\Psi(\boldsymbol{x}, \boldsymbol{\Omega}, s) =\\ &\delta(s)\left[\int_{4\pi}\int_0^\infty \frac{\nu c_f}{4\pi}\Sigma_t(\boldsymbol{\Omega}', s')\Psi(\boldsymbol{x}, \boldsymbol{\Omega}', s')ds'd\Omega'\right.\\ &\left.+\int_{4\pi}\int_0^\infty c_s P(\boldsymbol{\Omega}'\cdot\boldsymbol{\Omega})\Sigma_t(\boldsymbol{\Omega}', s')\Psi(\boldsymbol{x}, \boldsymbol{\Omega}', s')ds'd\Omega'\right].\end{aligned} \tag{2.16}$$

Finally, dividing the fission term by k_{eff} in Eq. (2.16) so as to guarantee the neutron balance, we obtain

$$\begin{aligned}&\frac{\partial}{\partial s}\Psi(\boldsymbol{x}, \boldsymbol{\Omega}, s) + \Sigma_t(\boldsymbol{\Omega}, s)\Psi(\boldsymbol{x}, \boldsymbol{\Omega}, s) + \boldsymbol{\Omega}\cdot\nabla\Psi(\boldsymbol{x}, \boldsymbol{\Omega}, s) =\\ &\delta(s)\left[\frac{1}{k_{eff}}\int_{4\pi}\int_0^\infty \frac{\nu c_f}{4\pi}\Sigma_t(\boldsymbol{\Omega}', s')\Psi(\boldsymbol{x}, \boldsymbol{\Omega}', s')ds'd\Omega'\right.\\ &\left.+\int_{4\pi}\int_0^\infty c_s P(\boldsymbol{\Omega}'\cdot\boldsymbol{\Omega})\Sigma_t(\boldsymbol{\Omega}', s')\Psi(\boldsymbol{x}, \boldsymbol{\Omega}', s')ds'd\Omega'\right],\end{aligned} \tag{2.17}$$

that is the k_{ell}-GLBE. Equation (2.17) can be rewritten in equivalent initial form, where the delta function $\delta(s)$ is not presented. For $s > 0$

Eq. (2.17) becomes

$$\frac{\partial}{\partial s}\Psi(\boldsymbol{x},\boldsymbol{\Omega},s)+\Sigma_t(\boldsymbol{\Omega},s)\Psi(\boldsymbol{x},\boldsymbol{\Omega},s)+\boldsymbol{\Omega}\cdot\nabla\Psi(\boldsymbol{x},\boldsymbol{\Omega},s)=0. \tag{2.18a}$$

Now, applying the operator

$$\lim_{\xi\to 0}\int_{-\xi}^{\xi}(\cdot)\,ds$$

on Eq. (2.17) and considering $\Psi=0$ for $s<0$ in the resulting equation, we obtain

$$\begin{aligned}\Psi(\boldsymbol{x},\boldsymbol{\Omega},0)=&\frac{1}{k_{eff}}\int_{4\pi}\int_0^{\infty}\frac{\nu c_f}{4\pi}\Sigma_t(\boldsymbol{\Omega}',s')\Psi(\boldsymbol{x},\boldsymbol{\Omega}',s')ds'd\Omega'\\&+\int_{4\pi}\int_0^{\infty}c_s P(\boldsymbol{\Omega}'\cdot\boldsymbol{\Omega})\Sigma_t(\boldsymbol{\Omega}',s')\Psi(\boldsymbol{x},\boldsymbol{\Omega}',s')ds'd\Omega.\end{aligned} \tag{2.18b}$$

Equations (2.18) are the initial value form of the k_{eff}-GLBE. In the next section we describe a solution scheme for the k_{eff}-GLBE.

3. A solution technique for the one-dimensional k_{eff}-GLBE in the S_N formulation

Let us consider the slab-geometry k_{eff}-GLBE in the S_N formulation (Lewis and Miller, 1993) with isotropic scattering. That is,

$$\frac{\partial}{\partial s}\Psi_n(z,s)+\mu_n\frac{\partial}{\partial z}\Psi_n(z,s)+\Sigma_{t_n}(s)\Psi_n(z,s)=0, \tag{3.1a}$$

$$\Psi_n(z,0)=\left(\frac{\nu c_f}{k_{eff}}+c_s\right)\sum_{n'=1}^{\mathrm{N}}\frac{\omega_{n'}}{2}\int_0^{\infty}\Sigma_{t_{n'}}(s')\Psi_{n'}(z,s')ds', \tag{3.1b}$$

where μ_n is a discrete direction of flight, such that $n=1,2,\ldots,\mathrm{N}$, with N being the order of the Gauss–Legendre quadrature with weights ω_n (Lewis and Miller, 1993). Moreover, $\Sigma_{t_n}(s)=\Sigma_t(\mu_n,s)$ and $\Psi_n(z,s)=\Psi(z,\mu_n,s)$.

3.1. Spectral approach

To deal with the s-dependence of Eqs. (3.1) we consider the Spectral Approach (SA) (Vasques et al., 2020). Following the SA, we leverage the orthogonal properties of the Laguerre polynomials concerning the inner product (Golderg et al., 1964)

$$\int_0^{\infty}e^{-s}L_m(s)L_{m'}(s)ds=\delta_{m,m'}, \tag{3.2a}$$

to write the angular flux as the following truncated Laguerre series

$$\Psi_n(z,s)=e^{-\int_0^s\Sigma_{t_n}(s')ds'}\sum_{m=0}^{\mathrm{M}}L_m(s)\phi_{n,m}(z). \tag{3.2b}$$

In Eqs. (3.2), $L_m(s)$ and $L_{m'}(s)$ are the Laguerre polynomials of order m and m' respectively, $\delta_{m,m'}$ is the Kronecker delta, and M is the truncation order of the Laguerre series. To represent the angular flux as given in Eq. (3.2b) one needs to obtain an expression for the Laguerre moments $\phi_{n,m}(z)$.

A set of equations for the Laguerre moments can be derived from Eqs. (3.1). First, we define the angular flux as

$$\Psi_n(z,s)=\psi_n(z,s)e^{-\int_0^s\Sigma_{t_n}(s')ds'}, \tag{3.3}$$

and substitute Eq. (3.3) into Eqs. (3.1) to obtain

$$\frac{\partial}{\partial s}\psi_n(z,s)+\mu_n\frac{\partial}{\partial z}\psi_n(z,s)=0, \tag{3.4a}$$

$$\psi_n(z,0)=\left(\frac{\nu c_f}{k_{eff}}+c_s\right)\sum_{n'=1}^{\mathrm{N}}\frac{\omega_{n'}}{2}\int_0^{\infty}p_{n'}(s')\psi_{n'}(z,s')ds', \tag{3.4b}$$

where

$$p_{n'}(s')=\Sigma_{t_{n'}}(s')e^{-\int_0^{s'}\Sigma_{t_{n'}}(s'')ds''} \tag{3.4c}$$

is the free-path distribution function in the discrete direction $\mu_{n'}$. Now, we represent $\psi_n(z,s)$ as the following truncated Laguerre series

$$\psi_n(z,s)=\sum_{m=0}^{\mathrm{M}}L_m(s)\phi_{n,m}(z), \tag{3.5}$$

where

$$\phi_{n,m}(z)=\int_0^{\infty}e^{-s}L_m(s)\psi_n(z,s)ds,$$

and we substitute Eq. (3.5) into Eqs. (3.4), thus obtaining

$$\sum_{m=0}^{\mathrm{M}}\phi_{n,m}(z)\frac{d}{ds}L_m(s)+\mu_n\sum_{m=0}^{\mathrm{M}}L_m(s)\frac{d}{dz}\phi_{n,m}(z)=0, \tag{3.6a}$$

$$\sum_{m=0}^{\mathrm{M}}\phi_{n,m}(z)=\left(\frac{\nu c_f}{k_{eff}}+c_s\right)\sum_{n'=1}^{\mathrm{N}}\frac{\omega_{n'}}{2}\sum_{m'=0}^{\mathrm{M}}\phi_{n',m'}(z)\mathcal{L}_{n',m'}, \tag{3.6b}$$

where

$$\mathcal{L}_{n',m'}=\int_0^{\infty}p_{n'}(s')L_{m'}(s')ds'. \tag{3.6c}$$

Operating Eq. (3.6a) with $\int_0^{\infty}e^{-s}(\cdot)ds$, and using that the Laguerre polynomials satisfy the relation $\frac{d}{ds}L_m(s)=\left(\frac{d}{ds}-1\right)L_{m-1}(s)$ for $m>0$ (Golderg et al., 1964), we obtain

$$\mu_n\frac{d}{dz}\phi_{n,m}(z)=\sum_{j=m+1}^{\mathrm{M}}\phi_{n,j}(z). \tag{3.7}$$

The left-hand side of Eq. (3.6b) can be split in a sum of two terms, one term being the right-hand side of Eq. (3.7), and the other being a summation of the moments $\phi_{n,j}(z)$ with j varying from 0 to m. Based on this, we substitute Eq. (3.6b) into Eq. (3.7) to obtain

$$\begin{aligned}&\mu_n\frac{d}{dz}\phi_{n,m}(z)+\sum_{j=0}^{m}\phi_{n,j}(z)=\\&\left(\frac{\nu c_f}{k_{eff}}+c_s\right)\sum_{n'=1}^{\mathrm{N}}\frac{\omega_{n'}}{2}\sum_{m'=0}^{\mathrm{M}}\phi_{n',m'}(z)\mathcal{L}_{n',m'},\ \begin{cases}n=1,2,\ldots,\mathrm{N}\\m=0,1,\ldots,\mathrm{M}\end{cases}.\end{aligned} \tag{3.8}$$

By using the SA, we can solve nonclassical problems through the solution of a "classical"-like system of equations, i.e., Eq. (3.8). Here the term "classical" is used to emphasize that the solution of Eq. (3.8) is not explicitly dependent of the variable s. The system of equations given in Eq. (3.8) is suitable for the use of current deterministic numerical methods, such as the well-known Diamond Difference method (Lewis and Miller, 1993), which will be given next.

3.2. Diamond difference method and the source iteration scheme

Let us consider the spatial domain (V) as composed of discrete spatial cells V_i, such that $V=\bigcup_{i=1}^{I}V_i$. Figure 1 illustrates the discretized spatial domain.

Operating Eq. (3.8) with $\frac{1}{h_i}\int_{z_{i-1/2}}^{z_{i+1/2}}(\cdot)dz$, we obtain the discretized spatial balance equation

$$\begin{aligned}&\frac{\mu_n}{h_i}\left[\phi_{n,m,i+1/2}-\phi_{n,m,i-1/2}\right]+\sum_{j=0}^{m}\overline{\phi}_{n,m,i}\\&=\left(\frac{\nu c_f}{k_{eff}}+c_s\right)\sum_{n'=1}^{\mathrm{N}}\frac{\omega_{n'}}{2}\sum_{m'=0}^{\mathrm{M}}\overline{\phi}_{n',m',i}\mathcal{L}_{n',m'},\end{aligned} \tag{3.9}$$

where $\phi_{n,m,i\pm1/2}=\phi_{n,m}(z_{i\pm1/2})$ and

$$\overline{\phi}_{n,m,i}=\frac{1}{h_i}\int_{z_{i-1/2}}^{z_{i+1/2}}\phi_{n,m}(z)dz,$$

is the cell-average Laguerre moment of order m. As with the Diamond Difference (DD) numerical method, we approximate $\phi_{n,m}(z)$ as piecewise continuous linear functions across the spatial grid, which is equivalent to considering

$$\overline{\phi}_{n,m,i}=\frac{\phi_{n,m,i+1/2}+\phi_{n,m,i-1/2}}{2}. \tag{3.10}$$

By substituting Eq. (3.10) into Eq. (3.9), we obtain two sets of equations for $\mu_n>0$ and for $\mu_n<0$. That is,

$$\phi_{n,m,i+1/2}=\frac{\left(\frac{1}{2}-\frac{\mu_n}{h_i}\right)\phi_{n,m,i-1/2}-\sum_{j=0}^{m}\overline{\phi}_{n,j,i}+\left(\frac{\nu c_f}{k_{eff}}+c_s\right)\Phi_i}{\left(\frac{1}{2}+\frac{\mu_n}{h_i}\right)},\ \mu_n>0,$$

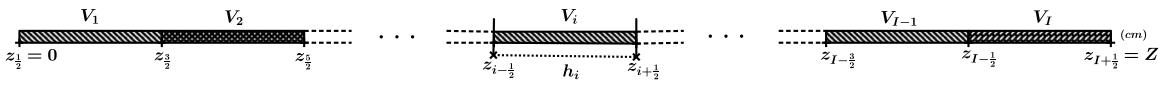

Fig. 1. Discretized spatial domain.

(3.11a)

$$\phi_{n,m,i-1/2} = \frac{\left(\frac{1}{2} - \frac{|\mu_n|}{h_i}\right)\phi_{n,m,i+1/2} - \sum_{j=0}^{m}\overline{\phi}_{n,j,i} + \left(\frac{\nu c_f}{k_{eff}} + c_s\right)\Phi_i}{\left(\frac{1}{2} + \frac{|\mu_n|}{h_i}\right)}, \ \mu_n < 0, \tag{3.11b}$$

where we have defined

$$\Phi_i = \sum_{n'=1}^{\mathrm{N}} \frac{\omega_{n'}}{2} \sum_{m'=0}^{\mathrm{M}} \overline{\phi}_{n',m',i}\mathcal{L}_{n',m'}. \tag{3.11c}$$

Equations (3.11) are the nonclassical S_N sweeping equations. We set $m = 0$ and use Eq. (3.11a) to sweep from left to right ($\mu_n > 0$) and Eq. (3.11b) to sweep from right to left ($\mu_n < 0$), updating in each sweep the values of $\overline{\phi}_{n,m,i}$. We follow this sweeping process from $m = 0$ to $m = \mathrm{M}$. Once all full values of $\overline{\phi}_{n,m,i}$ are calculated, we update function Φ_i (Eq. (3.11c)), and restart the sweeping process. This procedure is executed until the relative deviation between two consecutive estimates of Eq. (3.11c), for each value of i, is smaller than or equal to a prescribed positive number ξ. In other words, the sweeping process is executed until

$$\frac{\left|\Phi_i^{(\ell+1)} - \Phi_i^{(\ell)}\right|}{\Phi_i^{(\ell+1)}} \leq \xi, \ i = 1, 2, \ldots, I,$$

where the superscripts ℓ and $\ell + 1$ indicate two consecutive estimates of Φ_i. By using Eq. (3.2) together with Eqs. (3.11), we obtain numerical results for the k_{eff}-GLBE (Eqs. (3.1)) for a given estimate of k_{eff} in the power iteration method (Booth, 2006; Prinja and Larsen, 2010; Lewis and Miller, 1993).

3.3. Estimation of k_{eff}

Multiplication eigenvalue problems are traditionally solved by the method of power iteration (Alvim, 2007). Upon convergence, it is expected that

$$\frac{1}{k_{eff}^{(\ell^\star+1)}}\mathcal{F}^{(\ell^\star+1)} = \frac{1}{k_{eff}^{(\ell^\star)}}\mathcal{F}^{(\ell^\star)}, \ \ell^\star = 0, 1, 2, \ldots, \tag{3.12a}$$

where we have defined

$$\mathcal{F}^{(\ell^\star)} = \nu c_f \sum_{i=1}^{I}\sum_{n=1}^{\mathrm{N}}\sum_{m=0}^{\mathrm{M}} \omega_n \overline{\phi}_{n,m,i}^{(\ell^\star)}\mathcal{L}_{n,m}. \tag{3.12b}$$

In Eqs. (3.12), the superscript $(\ell^\star + 1)$ in $\mathcal{F}^{(\ell^\star+1)}$ indicates that $\overline{\phi}_{n,m,i}^{(\ell^\star+1)}$ is the converged cell-average Laguerre moment for $k_{eff} = k_{eff}^{(\ell^\star)}$ in Eqs. (3.11).

To estimate the value of $k_{eff}^{(1)}$ we make initial guesses for $k_{eff}^{(0)}$ and $\mathcal{F}^{(0)}$; then, we execute the sweeping process described in Section 3.2 with $k_{eff} = k_{eff}^{(0)}$ in order to evaluate $\mathcal{F}^{(1)}$. Then, we use $k_{eff}^{(0)}$, $\mathcal{F}^{(0)}$ and $\mathcal{F}^{(1)}$ to calculate the new estimate for k_{eff} , i.e., $k_{eff}^{(1)}$ through Eq. (3.12a). This procedure continues until the stop criterion

$$\frac{\left|k_{eff}^{(\ell^\star+1)} - k_{eff}^{(\ell^\star)}\right|}{k_{eff}^{(\ell^\star+1)}} \leq \rho, \ \ell^\star = 0, 1, 2, \ldots, \tag{3.13}$$

is satisfied, with ρ being a positive number.

4. Numerical results

In this section, we present numerical results for two different model problems. In the first model problem, we focus our attention on the estimate of k_{eff} in a classical transport problem, making use of the mathematical model and solution process described in this work. The point of considering a classical problem is to analyze the accuracy of the solution process. As will be shown later in this section, the k_{eff}-GLBE can be reduced to the linear Boltzmann equation for eigenvalue problems (k_{eff}-LBE) (Lewis and Miller, 1993) when $\Sigma_t(\mu, s) = \Sigma_t$. The k_{eff}-LBE is shown next

$$\mu\frac{\partial}{\partial z}\Psi^c(z,\mu) + \Sigma_t\Psi^c(z,\mu) = \frac{1}{2}\left(\frac{\nu\Sigma_f}{k_{eff}} + \Sigma_s\right)\int_{-1}^{1}\Psi^c(z,\mu')d\mu', \tag{4.1}$$

where Ψ^c is the classical neutron angular flux, and Σ_s and Σ_f are the scattering and fission macroscopic cross-sections respectively. As the k_{eff}-GLBE can be reduced to the k_{eff}-LBE, highly accurate results are expected for classical transport problems through the solution of Eqs. (3.1), thus ensuring the accuracy of the solution process.

After analyzing the accuracy of the solution process, we consider a nonclassical transport problem in model-problem II to examine the accuracy of the solution generated using the nonclassical model. To compare the results generated by the nonclassical model, we solve the same nonclassical problem by making use of the direct method. That is, a sufficient number of physical realizations of the system is generated, and the k_{eff} and the profile of the classical neutron scalar flux are calculated for each physical realization through the solution of the k_{eff}-LBE. The expected value of k_{eff} and the expected profile of the neutron scalar flux are calculated through the average of the solutions generated in each physical realization.

For all numerical experiments we consider $\xi = \rho = 1 \times 10^{-7}$ for the stopping criteria. Moreover, we adopt $N = 20$ in the S_N formulation, $\mathrm{M} = 100$ in the expansion of the angular flux as a Laguerre series, and we discretize the spatial domain such that $h_i = 0.01\ cm$ for $i = 1 : I$.

4.1. Model-problem I

In the first model problem, we consider a classical transport problem with size $Z = 30$ cm. To model this problem, we consider the total cross-section uniform concerning variables μ and s. In this case, the function $\mathcal{L}_{n',m'}$ (Eq. (3.6c)) is reduced to

$$\mathcal{L}_{n',m'} = \Sigma_t\int_0^\infty e^{-\Sigma_t s'}L_{m'}(s')ds'. \tag{4.2}$$

Substituting the representation for the Laguerre polynomials (Golderg et al., 1964)

$$L_{m'}(s') = \sum_{j=0}^{m'}(-1)^j\binom{m'}{j}\frac{s'^j}{j!}$$

into Eq. (4.2), and considering the result

$$\int_0^\infty e^{-s}s'^j\,ds' = j!,$$

we write

$$\mathcal{L}_{n',m'} = \sum_{j=0}^{m'}\left(\frac{-1}{\Sigma_t}\right)^j\binom{m'}{j}. \tag{4.3a}$$

Equation (4.3a) can be rewritten using the binomial theorem as (Yang, 2017)

$$\mathcal{L}_{n',m'} = \left(1 - \frac{1}{\Sigma_t}\right)^{m'}. \tag{4.3b}$$

Table 1
k_{eff} and profile of the classical neutron scalar flux for model-problem I.

Material parameters			k_{eff}	Profile of the classical particle flux[a]			
				z[b] = 0	$z = 5$	$z = 10$	$z = 15$
$\Sigma_t = 0.5$	$c_s = 0.2$	$\nu c_f = 0.1$	0.123136 (−1.31E−07[c])	0.025955 (−4.85E−06[d])	0.137132 (−4.74E−05)	0.211584 (−1.76E−06)	0.238399 (−1.98E−06)
		$\nu c_f = 0.6$	0.738815 (−1.30E−07)				
	$c_s = 0.5$	$\nu c_f = 0.1$	0.195270 (−1.97E−07)	0.041158 (−5.41E−06)	0.217458 (−4.77E−05)	0.335534 (−1.75E−06)	0.378050 (−1.83E−06)
		$\nu c_f = 0.6$	1.171622 (−1.97E−07)				
$\Sigma_t = 1.3$	$c_s = 0.1$	$\nu c_f = 0.1$	0.110863 (−3.52E−08)	0.003864 (−3.16E−06)	0.045948 (−2.58E−06)	0.075514 (7.20E−07)	0.086218 (2.34E−06)
		$\nu c_f = 0.3$	0.332588 (−3.52E−08)				
	$c_s = 0.7$	$\nu c_f = 0.1$	0.331113 (8.65E−09)	0.011544 (−4.03E−06)	0.137051 (−2.45E−06)	0.225614 (6.85E−07)	0.257802 (2.21E−06)
		$\nu c_f = 0.3$	0.993340 (8.65E−09)				
$\Sigma_t = 3$	$c_s = 0.3$	$\nu c_f = 0.2$	0.285547 (−9.01E−08)	0.001012 (−8.29E−05)	0.025834 (−2.81E−05)	0.042473 (1.27E−06)	0.049107 (4.88E−06)
		$\nu c_f = 0.35$	0.499708 (−9.01E−08)				
	$c_s = 0.6$	$\nu c_f = 0.2$	0.499502 (−1.24E−07)	0.001725 (4.50E−05)	0.044478 (2.13E−05)	0.074569 (−8.97E−06)	0.085297 (−3.83E−05)
		$\nu c_f = 0.35$	0.874129 (−1.24E−07)				

[a] The classical neutron scalar flux is generated through the nonclassical solution as $\Phi^c(z) = \int_{-1}^{1}\int_0^\infty \Psi(z,\mu,s)ds\,d\mu$ $neutrons/cm^2 s$.
[b] Since this is a symmetric problem, $z = a\,cm$ represents the profile of the classical scalar flux at $z = a\,cm$ and $z = 30 - a\,cm$.
[c] The relative deviation of k_{eff} generated by Eqs. (3.1) and (4.1).
[d] The relative deviation of the profile of the classical neutron scalar flux generated by Eqs. (3.1) and (4.1).

Once the function $\mathcal{L}_{n',m'}$ is calculated, we use the nonclassical formulation to solve different classical problems, varying Σ_t, c_s and νc_f. Table 1 presents the multiplication factor k_{eff} as generated by the solution of Eqs. (3.1) and by the solution of Eq. (4.1). To solve Eq. (4.1) we use the S_N formulation and the DD method to deal with the angular and spatial variables, respectively, and the power iteration method to estimate k_{eff}. The values for the stopping criterion, quadrature order, and the number of discretization nodes are considered the same as in the solution of Eqs. (3.1). Furthermore, Table 1 and Fig. 2 present the profile of the classical scalar flux in some points of the spatial domain.

At this point, we remark that using the same methods to solve both Eqs. (3.1) and (4.1) does not impose any concerning the validity of the generated results. The methods used to solve Eq. (4.1) have been used over decades in the nuclear engineering area to calculate k_{eff}, always showing good accuracy when compared to results generated by other methods, such as the Response Matrix method (da Silva et al., 2020; Moraes et al., 2020a,b, 2023a) and the Spectral Green's Function method (Menezes et al., 2013; de Abreu et al., 1996; Barros et al., 2003). The results generated using these methods have been used as benchmarks in several different articles. Therefore, by solving Eq. (4.1) using these methods we expected to obtain the exact results for k_{eff} and the profile of scalar flux within the precision defined by the stopping criteria.

As we can see from Table 1 and Fig. 2, the results generated by the nonclassical model were highly accurate for classical transport problems. All estimations of k_{eff} generated by the solution of Eqs. (3.1) agree up to 7 digits of precision (comparable with the stopping criteria) with the results generated by the solution of Eq. (4.1), while the profile of the scalar flux agrees at least 5 digits of precision (a slight loss of precision compared to the stopping criterion). This is a strong indication that the solution process described in Section 3 is adequate to generate very accurate results. We remark that the accuracy of the generated solution depends not only on the solution process but also on the right consideration of the homogenized total-cross section $\Sigma_t(\mu, s)$.

As briefly stated in the beginning of this section, these highly accurate results were in fact expected, since Eqs. (3.1) can be reduced to Eq. (4.1). Considering $\Sigma_t(\mu, s) = \Sigma_t$ in Eqs. (3.1), and then operating the resulting equation by $\int_0^\infty(\cdot)ds$ we obtain

$$\Psi_n(z,0) + \mu_n \frac{d}{dz}\Psi_n^c(z) + \Sigma_t \Psi_n^c(z) = 0, \tag{4.4}$$

where the classical neutron angular flux is defined as

$$\Psi_n^c(z) = \int_0^\infty \Psi_n(z,s)ds.$$

Substituting Eq. (3.1b) into Eq. (4.4) we obtain

$$\mu_n \frac{d}{dz}\Psi_n^c(z) + \Sigma_t \Psi_n^c(z) = \frac{1}{2}\left(\frac{\nu\Sigma_f}{k_{eff}} + \Sigma_s\right)\sum_{n'=1}^{N}\omega_{n'}\Psi_{n'}^c(z), \tag{4.5}$$

which is the k_{eff}-LBE in the S_N formulation. In Eq. (4.5) $\Sigma_s = \Sigma_t\, c_s$ and $\Sigma_f = \Sigma_t\, c_f$.

4.2. Model-problem II

In the second model problem, we consider a stochastic problem constituted of two materials of length ℓ that are periodically arranged in the infinite line $-\infty < z < \infty$, as illustrated in Fig. 3.

The total macroscopic cross-section of material 1 is $\Sigma_t = \Sigma_{t_1}\ cm^{-1}$ and for material 2 is $\Sigma_{t_2} = 0$ (void). We have opted to consider this nonclassical problem due to the fact that the free-path distribution function (Eq. (3.4c)) can be analytically calculated in this case. The function $p_{n'}(s')$ for this problem is

$$p_{n'}(s') = \begin{cases} \frac{\Sigma_{t_1}}{\ell}\left[\ell(2d+1) - s'|\mu_{n'}|\right] e^{-\Sigma_{t_1}\left(s' - \frac{d\ell}{|\mu_{n'}|}\right)}, \\ \text{if } 2d\ell \le s'|\mu_{n'}| \le (2d+1)\ell \\ \frac{\Sigma_{t_1}}{\ell}\left[s'|\mu_{n'}| - \ell(2d+1)\right] e^{-\Sigma_{t_1}\left(s' - \frac{(d+1)\ell}{|\mu_{n'}|}\right)}, \\ \text{if } (2d+1)\ell \le s'|\mu_{n'}| \le 2(d+1)\ell \end{cases}, \tag{4.6}$$

where $d = 0, 1, 2, \ldots$. Details about the constitution of Eq. (4.6) can be found in Vasques et al. (2020, 2017).

The calculation of function $\mathcal{L}_{n',m'}$ is a complicated task in this problem given the constitution of the function $p_{n'}(s')$. Thus, we use a numerical approach to calculate function $\mathcal{L}_{n',m'}$. In this numerical approach, we first truncate the upper limit of variable s' to a finite number S in Eq. (3.6c) and neglect the integral in the complementary range (S, ∞). Then, we consider the simple transformation $q = \frac{2}{S}s' - 1$ in the resulting integral, which changes the interval of integration from $[0, S]$ to $[-1, 1]$. Finally, we use the Gauss–Legendre quadrature formula to obtain

$$\mathcal{L}_{n',m'} \approx \frac{S}{2}\sum_{k=1}^{G\ell} p_{n'}\left(\frac{S}{2}(q_k+1)\right) L_{m'}\left(\frac{S}{2}(q_k+1)\right)\omega_k, \tag{4.7}$$

where q_k and ω_k are, respectively, the nodes and weights of the Gauss–Legendre angular quadrature of order $G\ell$. As the calculation of the function $\mathcal{L}_{n',m'}$ is essential to the generation of accurate results for k_{eff}

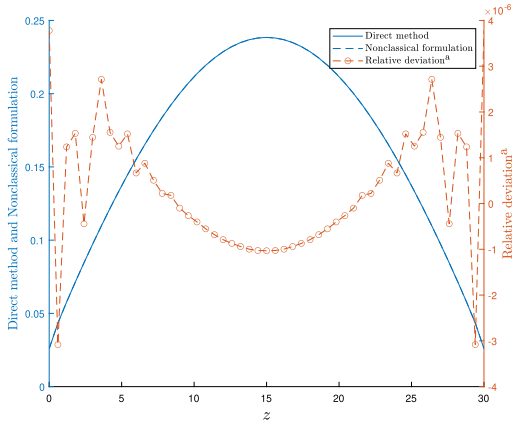

(a) $\Sigma_t = 0.5\,cm^{-1}$, $c_s = 0.2$, and $\nu c_f = 0.1$.

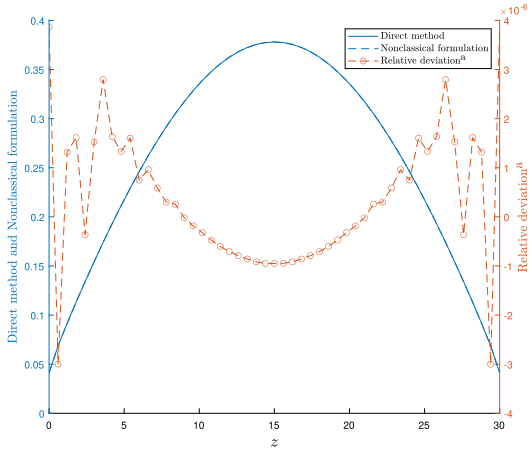

(b) $\Sigma_t = 0.5\,cm^{-1}$, $c_s = 0.5$, and $\nu c_f = 0.1$.

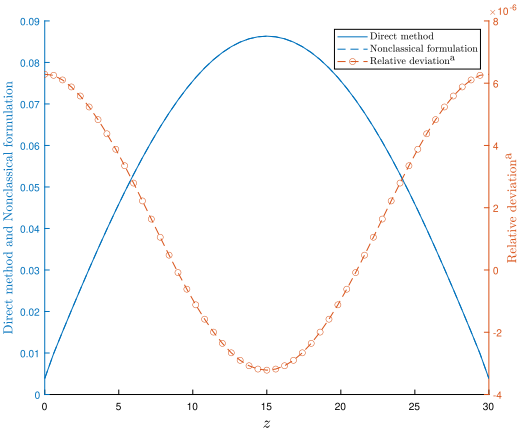

(c) $\Sigma_t = 1.3\,cm^{-1}$, $c_s = 0.1$, and $\nu c_f = 0.1$.

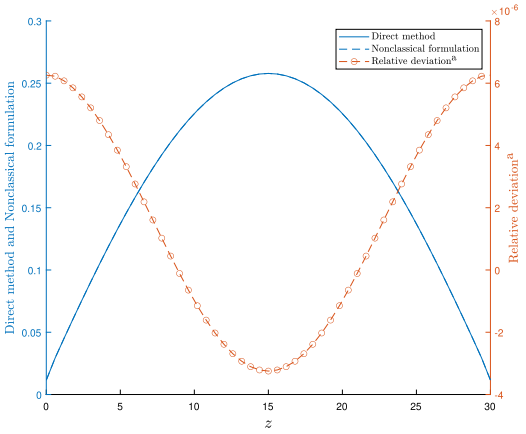

(d) $\Sigma_t = 1.3\,cm^{-1}$, $c_s = 0.7$, and $\nu c_f = 0.1$.

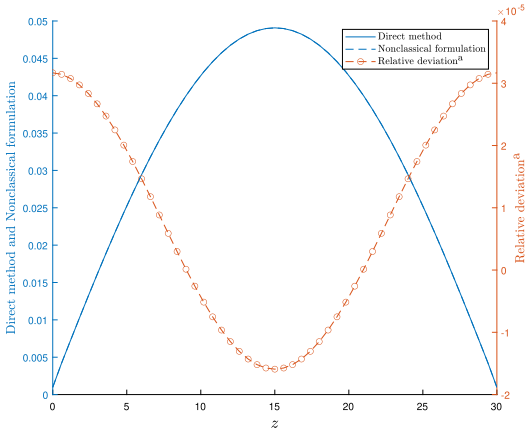

(e) $\Sigma_t = 3\,cm^{-1}$, $c_s = 0.3$, and $\nu c_f = 0.2$.

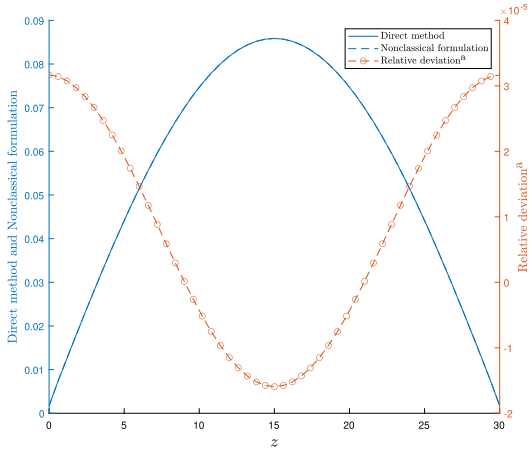

(f) $\Sigma_t = 3\,cm^{-1}$, $c_s = 0.6$, and $\nu c_f = 0.2$.

[a] The relative deviation between the solutions generated by the Direct method and Nonclassical formulation.

Fig. 2. Profile of the classical particle flux of model-problem I.

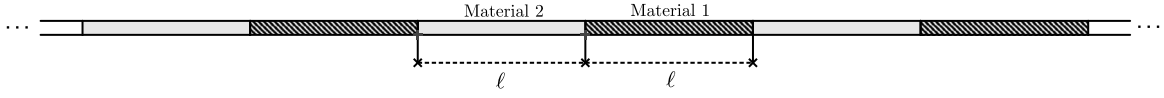

Fig. 3. Model-problem II: One-dimensional random periodic media.

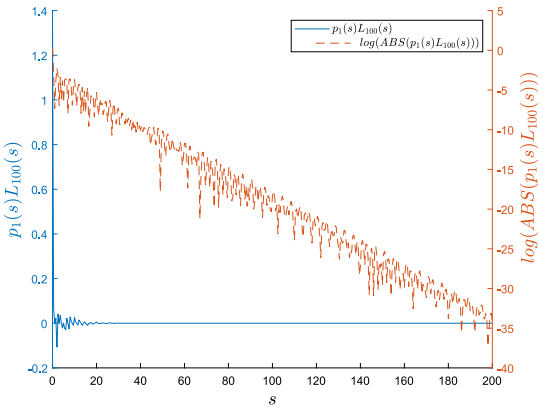

(a) $p_1(s)L_{100}(s)$ with $\Sigma_{t_1} = 1.3\,cm^{-1}$.

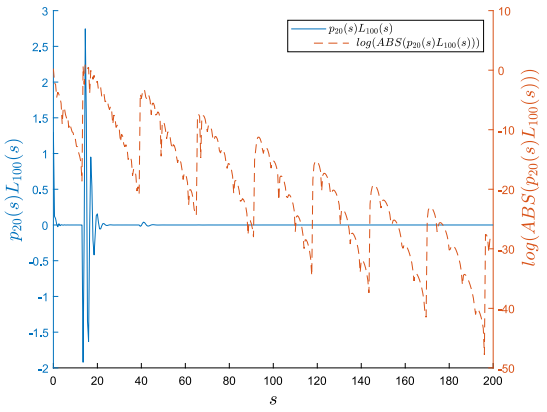

(b) $p_{20}(s)L_{100}(s)$ with $\Sigma_{t_1} = 1.3\,cm^{-1}$.

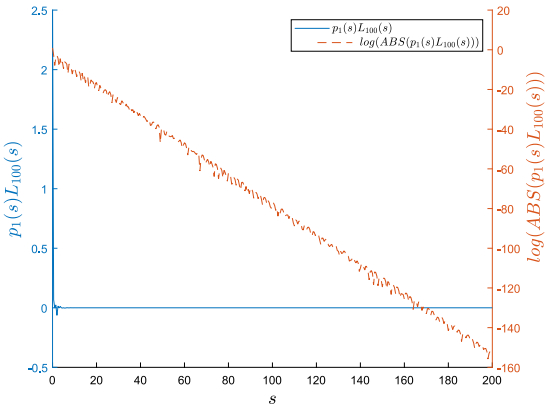

(c) $p_1(s)L_{100}(s)$ with $\Sigma_{t_1} = 2.5\,cm^{-1}$.

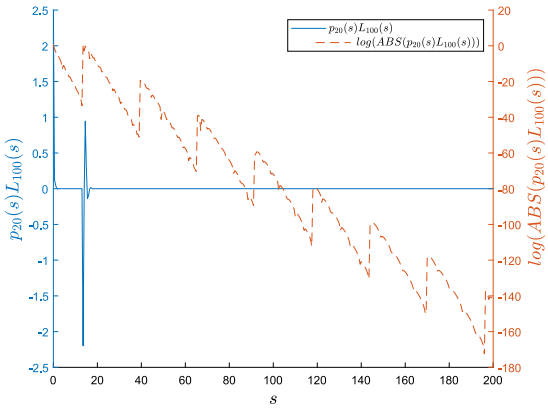

(d) $p_{20}(s)L_{100}(s)$ with $\Sigma_{t_1} = 2.5\,cm^{-1}$.

Fig. 4. Convergence of functions $\mathcal{L}_{n',m'}$ for model-problem II.

and the profile of the classical scalar flux following the solution process given in Section 3, we consider a high value for $G\ell = 6000$.

After we have defined a procedure to calculate functions $\mathcal{L}_{n',m'}$ for this nonclassical problem, we use the procedure described in Section 3 to calculate k_{eff}. We perform numerical experiments for different values of Z, Σ_{t_1}, c_s and νc_f, and compare the results with the results generated by the direct method as can be seen in Table 2 and Fig. 5. The solution generated by the direct method is the average of the solutions of the k_{eff}-LBE for 1000 classical transport problems varying the problem's configuration accordingly (Vasques et al., 2017).

As with the results displayed in Table 2 and Fig. 5 we have considered $S = 200$ cm in Eq. (4.7) to approximate functions $\mathcal{L}_{n',m'}$. By using Eq. (4.7) to calculate functions $\mathcal{L}_{n',m'}$, it is important to make sure that the function $p_{n'}(s)L_{m'}(s)$ converges for all possible values of n' and m', and to chose S such that the integral in the complementary range $[S, \infty]$ is close to zero. To visualize these features, we display in Fig. 4 the profile of function $p_{n'}(s)L_{m'}(s)$ considering $\mu_1 = 0.993126$, $\mu_{20} = -0.076526$, $m' = 100$, and $S \leq 200$ cm for the cases $\Sigma_{t_1} = 1.3\,\text{cm}^{-1}$ and $\Sigma_{t_1} = 2.5\,\text{cm}^{-1}$. Here, μ_1 and μ_{20} are the discrete directions with maximum and minimum absolute value, respectively, and $L_{100}(s)$ is the Laguerre polynomial of maximum order.

Analyzing Fig. 4, we can notice that the functions $p_1(s)L_{100}(s)$ and $p_{20}(s)L_{100}(s)$ go to zero with the increase of s, which indicates that the improper integral presented in Eq. (3.6c) converges for the $p_{n'}(s)$ displayed in Eq. (4.6) with $\Sigma_{t_1} = 1.3\,\text{cm}^{-1}$ and $\Sigma_{t_1} = 2.5\,\text{cm}^{-1}$. Moreover, these functions go to zero quickly with the increase of s. We chose $S = 200$ cm due to the fact that functions $p_1(s)L_{100}(s)$ and $p_{20}(s)L_{100}(s)$ with $\Sigma_{t_1} = 1.3\,\text{cm}^{-1}$ and $\Sigma_{t_1} = 2.5\,\text{cm}^{-1}$ are smaller than 1×10^{-15} (double precision digits) from now on.

As we can notice from Table 2, the nonclassical formulation has generated results for k_{eff} that agree from 2 to 5 decimal places with the expected value of k_{eff} generated by the direct method. The value of k_{eff} generated by the solution of Eqs. (3.1) with functions $\mathcal{L}_{n',m'}$ given in Eq. (4.7) slightly underestimates the expected value of k_{eff}. Moreover, the estimate of k_{eff} becomes more accurate with the increase of the size of the domain (Z).

To explain these results, let us analyze Fig. 5. As we can see, the profile of the classical neutron scalar flux becomes more accurate near the center of the domain, while its accuracy deteriorates near the boundaries. In the derivation of Eqs. (2.18) and in the calculation of functions $p_{n'}(s')$, the system is considered infinite. Therefore, a loss of precision near the boundaries is expected, since we are dealing with finite problems. However, neutrons that migrate more deeply within in the system are more important to the constitution of k_{eff} than neutrons that migrate closer to the boundaries. The neutrons that are close to the boundaries have a higher probability of leaking out of the system, thus not contributing significantly to new fission events. Therefore, neutrons that migrate near the boundaries and contribute to fission events is significantly smaller than the neutrons that migrate more deeply within the system. Thus, although we lose some precision near boundaries, which could considerably decrease the accuracy of k_{eff}, the fact that these neutrons do not contribute significantly to the estimate of k_{eff} ensures that k_{eff} can be accurately calculated using the nonclassical formulation as presented in this paper.

This argument can also be applied to explain the improvement in the estimation of k_{eff} with the increase of the size of the domain. When we increase the size of the domain, considering the same cross-section, we decrease the number of particles near the boundaries. Thus,

Table 2
k_{eff} and profile of the classical neutron scalar flux for model-problem II.

Domain size	Material parameters			k_{eff}	Profile of the classical particle flux[a]			
					$z = 0$[b]	$z = 4$	$z = 8$	$z = 10$
$Z = 20$	$\Sigma_t = 1.3$	$c_s = 0.1$	$vc_f = 0.1$	0.109063 (−1.34E−03[c])	0.033196 (1.01E−01[d])	0.158880 (−2.28E−03)	0.230601 (−5.97E−03)	0.240122 (−6.30E−03)
			$vc_f = 0.3$	0.327188 (−1.34E−03)				
		$c_s = 0.7$	$vc_f = 0.1$	0.315555 (−3.86E−03)	0.096044 (9.90E−02)	0.459686 (−4.83E−03)	0.667215 (−8.49E−03)	0.694764 (−8.82E−03)
			$vc_f = 0.3$	0.946665 (−3.86E−03)				
	$\Sigma_t = 2.5$	$c_s = 0.1$	$vc_f = 0.1$	0.110400 (−1.21E−03)	0.011713 (−2.31E−01)	0.082774 (−1.35E−03)	0.124942 (−1.03E−02)	0.130570 (−1.11E−02)
			$vc_f = 0.3$	0.331202 (−1.21E−03)				
		$c_s = 0.7$	$vc_f = 0.1$	0.327022 (−3.58E−03)	0.034686 (−2.29E−01)	0.245162 (−3.84E−03)	0.370135 (−1.26E−02)	0.386821 (−1.34E−02)
			$vc_f = 0.3$	0.981067 (−3.58E−03)				
					$z = 0$	$z = 10$	$z = 20$	$z = 25$
$Z = 50$	$\Sigma_t = 1.3$	$c_s = 0.1$	$vc_f = 0.1$	0.110731 (−2.62E−04)	0.006128 (1.06E−01)	0.063702 (2.67E−04)	0.098009 (−2.29E−03)	0.102594 (−1.98E−03)
			$vc_f = 0.3$	0.332193 (−2.62E−04)				
		$c_s = 0.7$	$vc_f = 0.1$	0.329939 (−7.71E−04)	0.018241 (1.04E−01)	0.189730 (−6.62E−04)	0.292137 (−2.44E−03)	0.305844 (−2.00E−03)
			$vc_f = 0.3$	0.989817 (−7.71E−04)				
	$\Sigma_t = 2.5$	$c_s = 0.1$	$vc_f = 0.1$	0.110986 (−2.31E−04)	0.002053 (2.46E−01)	0.033173 (4.87E−03)	0.051666 (−7.34E−03)	0.054110 (−8.46E−03)
			$vc_f = 0.3$	0.332958 (−2.31E−04)				
		$c_s = 0.7$	$vc_f = 0.1$	0.332222 (−6.62E−04)	0.006089 (2.39E−01)	0.098896 (3.97E−04)	0.155168 (−4.45E−03)	0.162708 (−4.31E−03)
			$vc_f = 0.3$	0.996665 (−6.62E−04)				
					$z = 0$	$z = 20$	$z = 40$	$z = 50$
$Z = 100$	$\Sigma_t = 1.3$	$c_s = 0.1$	$vc_f = 0.1$	0.111010 (−8.48E−05)	0.001629 (1.20E−01)	0.031964 (7.14E−03)	0.049754 (−6.62E−03)	0.052084 (−8.89E−03)
			$vc_f = 0.3$	0.333029 (−8.48E−05)				
		$c_s = 0.7$	$vc_f = 0.1$	0.332436 (−2.17E−04)	0.004810 (1.07E−01)	0.095117 (7.03E−04)	0.149758 (−1.62E−03)	0.157076 (−1.94E−03)
			$vc_f = 0.3$	0.997308 (−2.17E−04)				
	$\Sigma_t = 2.5$	$c_s = 0.1$	$vc_f = 0.1$	0.111074 (−1.01E−04)	0.000599 (3.39E−01)	0.017565 (6.27E−02)	0.024879 (−5.67E−02)	0.025595 (−7.87E−02)
			$vc_f = 0.3$	0.333223 (−1.01E−04)				
		$c_s = 0.7$	$vc_f = 0.1$	0.333041 (−1.91E−04)	0.001591 (2.54E−01)	0.049776 (8.13E−03)	0.078199 (−8.08E−03)	0.081917 (−1.07E−02)
			$vc_f = 0.3$	0.999123 (−1.91E−04)				

[a] The classical neutron scalar flux is generated through the nonclassical solution as $\Phi^c(z) = \int_{-1}^{1}\int_0^{\infty}\Psi(z,\mu,s)ds\,d\mu$ $neutrons/cm^2s$.
[b] Since this is a symmetric problem $z = a\,cm$ represents the profile of the classical scalar flux at $z = a\,cm$ and $z = Z - a\,cm$.
[c] The relative deviation of k_{eff} generated by Eqs. Eq. (3.1) and (4.1).
[d] The relative deviation of the profile of the classical neutron scalar flux generated by Eq. (3.1) and (4.1).

neutrons that migrating near the boundaries possess less influence on the calculation of k_{eff}, thus increasing its accuracy. Analyzing Table 2 we can see that the most accurate results for k_{eff} are generated for problems whose profile of the classical neutron flux is smaller at the boundaries.

The consideration of an infinite system in the calculation of functions $p_{n'}(s')$ can also be used to explain the underestimation of the k_{eff} coefficient generated by the solution of Eqs. (3.1). To visualize this relation, let us first introduce the well-known expression for the particle mean free path (MFP), i.e., the average distance the particle travels between collisions with other moving particles (background material). That is,

$$\langle s_{n'}\rangle = \int_0^{\infty} s' p_{n'}(s')ds'. \tag{4.8a}$$

In the case of the $p_{n'}(s')$ function as given in Eq. (4.6), Eq. (4.8a) becomes

$$\langle s_{n'}\rangle = \langle s\rangle = \frac{2}{\Sigma_{t_1}}. \tag{4.8b}$$

As in the calculation of functions $p_{n'}(s')$ the system was considered infinite, it is possible for the functions $p_{n'}(s')$ to assume values different than zero for distances ($z = \mu_n s$) greater than the domain size Z. Regarding finite systems, the function $p_{n'}(s')$ should be zero for such distances since the particle will no longer be in the system, then the probability of its collision is zero. The fact that $p_{n'}(s')$ can be different than zero for distances greater than Z increases the particle MFP (Eq. (4.8a)). In this case, particles will migrate larger distances between collisions. That decreases the average number of collisions in the system and increases the probability of a particle leaking out. We remark that although the probability of a particle leaking out of the system increases, this does not necessarily mean that a larger number of particles will leak out of the system in the case of a longer MFP. As the number of particles near the boundaries decreases due to a smaller number of fission events, the actual number of particles leaking out of the system may decrease for a larger MPF, despite their higher probability of leaking out.

The decrease in the number of collisions in the system may lead to a change in the constitution of the effective multiplication factor of the system. Let us consider,

$$k^1_{eff} = \frac{X}{Y}, \tag{4.9a}$$

as the k_{eff} coefficient considering the right $p_{n'}(s')$. In Eq. (4.9a) X and Y are the number of neutrons generated through fission in two consecutive generations. Now, we assume a different $p_{n'}(s')$ that increases the particle MFP, for example, considering the system as infinite. We also assume that this higher MFP leads to a decrease ($D > 0$) in the number of neutrons generated through fission. To represent this situation, we subtract D of both X and Y in Eq. (4.9a), thus obtaining

$$k^2_{eff} = \frac{X - D}{Y - D} = \frac{X}{Y - D} - \frac{D}{Y - D}. \tag{4.9b}$$

Equation (4.9b) is an estimate of the k_{eff} coefficient for the $p_{n'}(s')$ with a higher MFP. If we multiply Eq. (4.9a) by $\frac{Y-D}{Y-D}$, and Eq. (4.9b) by $\frac{Y}{Y}$

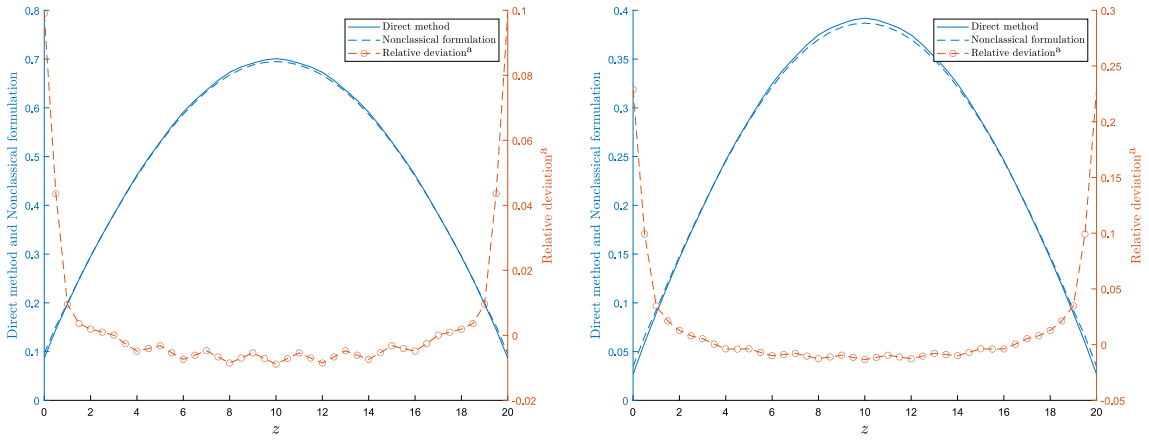

(a) $Z = 20\,cm$, $\Sigma_{t_1} = 1.3\,cm^{-1}$, $c_s = 0.7$, and $\nu c_f = 0.1$.

(b) $Z = 20\,cm$, $\Sigma_{t_1} = 2.5\,cm^{-1}$, $c_s = 0.7$, and $\nu c_f = 0.1$.

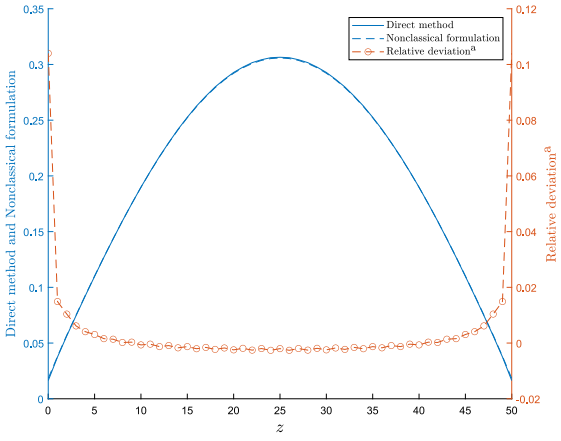

(c) $Z = 50\,cm$, $\Sigma_{t_1} = 1.3\,cm^{-1}$, $c_s = 0.7$, and $\nu c_f = 0.1$.

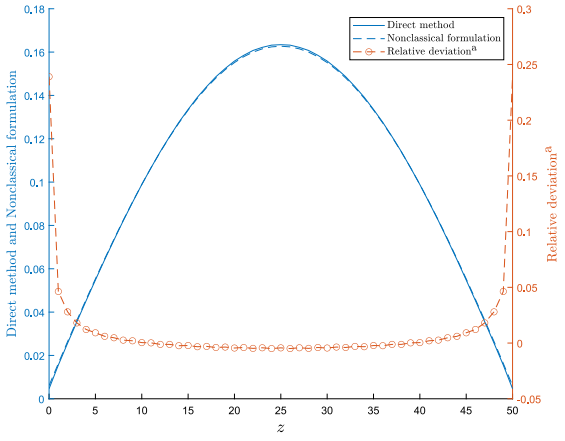

(d) $Z = 50\,cm$, $\Sigma_{t_1} = 2.5\,cm^{-1}$, $c_s = 0.7$, and $\nu c_f = 0.1$.

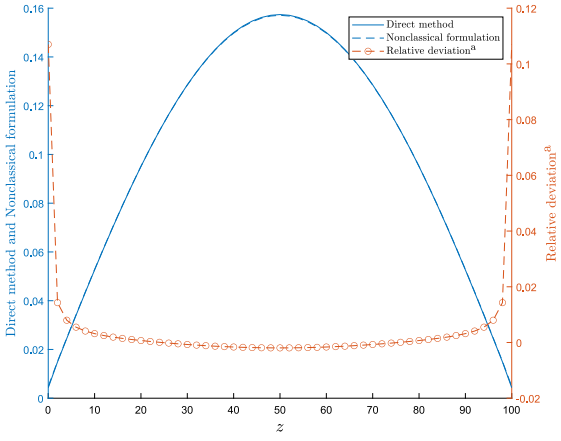

(e) $Z = 100\,cm$, $\Sigma_{t_1} = 1.3\,cm^{-1}$, $c_s = 0.7$, and $\nu c_f = 0.1$.

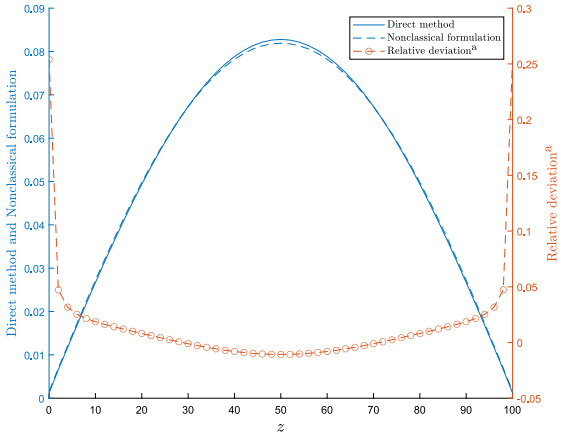

(f) $Z = 100\,cm$, $\Sigma_{t_1} = 2.5\,cm^{-1}$, $c_s = 0.7$, and $\nu c_f = 0.1$.

[a] The relative deviation between the solutions generated by the Direct method and Nonclassical formulation.

Fig. 5. Profile of the classical particle flux of model-problem II.

we obtain

$$k_{eff}^1 = \frac{XY}{(Y-D)\,Y} - \frac{X\,D}{(Y-D)\,Y}, \tag{4.10a}$$

and

$$k_{eff}^2 = \frac{XY}{(Y-D)\,Y} - \frac{Y\,D}{(Y-D)\,Y}, \tag{4.10b}$$

If the system is subcritical, it means that $Y > X$. Comparing Eq. (4.10a) to Eq. (4.10b), we can notice that in the case of subcritical system $k_{eff}^2 < k_{eff}^1$. Therefore, the k_{eff} coefficient for the case where $p_{n'}(s')$ overestimate the MFP is an underestimate of the k_{eff} coefficient for the right $p_{n'}(s')$. This idea can be used to explain the underestimating results presented in Table 2. At this point, we remark that the consideration of a $p_{n'}(s')$ that overestimates the MFP does not necessarily lead to a value $D > 0$ since both the number of collisions and particle leakage may decrease.

5. Concluding remarks

In this work, we derived a nonclassical transport equation to eigenvalue calculations (k_{eff}-GLBE). This derivation follows the idea of extending the phase-space of the total macroscopic cross-section to include the variables $\boldsymbol{\Omega}$ (particle's direction of flight) and s (distance traveled by the particle since its last interaction). It is demonstrated in Section 2 that this extension allows the mathematical modeling of transport problems where the flux of particles is not exponentially attenuated. The k_{eff}-GLBE is reduced to the classical transport equation, namely the linear Boltzmann equation, for eigenvalue calculations if classical transport takes place, as shown in the previous section.

To analyze the accuracy of the results generated through the solution of the k_{eff}-GLBE, we present numerical experiments for two one-dimensional model problems. In the first model problem, we consider a classical transport problem with the aim of examining the accuracy of the solution methodology described in Section 3. In model problem II, we consider the transport of neutrons in a random periodic media to analyze the accuracy of the derived nonclassical model. The results presented in the previous section indicate that the mathematical model derived in this work can generate accurate results for k_{eff} in nonclassical transport problems. The profile of the classical neutron scalar flux can also be calculated accurately (comparable to k_{eff}), although some precision near the problem's boundaries is lost. The assumption of an infinite system considered in the derivation of the k_{eff}-GLBE is one of the reasons for the behavior of the scalar flux profile. Thus, for nonclassical transport problems where the scalar flux profile needs to be calculated accurately in the whole domain, the assumption of a finite system in the derivation of the k_{eff}-GLBE should be considered. This is a subject for future work.

Another factor that has contributed to the loss of precision in the results generated in the second model problem of the previous section is the determination of functions $p_{n'}(s')$, and hence the constitution of the homogenized cross-section

$$\Sigma_t(\mu, s) = \frac{p(\mu, s)}{1 - \int_0^s p(\mu, s')ds'}.$$

In the derivation of the k_{eff}-GLBE, the true cross-section of the problem is replaced by a homogenized cross-section. Therefore, it is important given a nonclassical problem to consider a homogenized cross-section that can accurately portray the main characteristics of the problem. This importance is exemplified in the model problem I. In the model problem I, we have considered the homogenized cross-section as the true cross-section of the problem, which has led to the generation of highly accurate results for both k_{eff} and the profile of the scalar flux. Generating cross sections that accurately capture the statistical behavior of the medium in nonclassical transport problems of practical relevance is crucial and should be addressed in future work.

The constitution of the function $p_{n'}(s')$ can also impose numerical challenges concerning the method used to deal with the variable s. Regarding the Spectral Approach, the precise determination of the function $\mathcal{L}_{n',m'}$ is required to generate accurate results. However, depending on the constitution of $p_{n'}(s')$, the task of finding the analytical solution of the improper integral of Eq. (3.6c) is difficult (if not impossible), which foments the use of numerical methods to approximate this integral. By using numerical methods, we approximate the improper integral through the sum of the function $p_{n'}(s')L_{m'}(s')$ in some specified points. For nonclassical problems where $p_{n'}(s')$ has a long tail, i.e., it decreases smoothly with the increase of s, the function $p_{n'}(s')L_{m'}(s')$ can achieve very high values, following the image of the Laguerre polynomials. This situation can lead to numerical overflows. In the work (Moraes et al., 2022c), the authors have proposed a slight modification of the expansion of the particle flux as a Laguerre series (Eq. (3.2)) which can avoid this situation in some nonclassical problems. However, as the modification proposed in Moraes et al. (2022c) does not solve completely (for every nonclassical problem) this numerical issue, the exploration of different expansions for the flux of particles (considering other sets of polynomials) is of interest and should await future work.

In conjunction with the topics of future work already discussed in this section, we intend to continue this work by extending the mathematical model adopted here to multidimensional and multigroup calculations. Moreover, the implementation of acceleration schemes to improve the efficiency of the solution process is of great interest.

Declaration of competing interest

The authors declare that they have no known competing financial interests or personal relationships that could have appeared to influence the work reported in this paper.

Acknowledgments

This study was financed in part by Coordenação de Aperfeiçoamento de Pessoal de Nível Superior (CAPES) - Brasil - Finance Code 001, and Conselho Nacional de Desenvolvimento Científico e Tecnológico (CNPq) – Brasil (CNPq - Processo 170605/2023-0). R.C. Barros also acknowledges support from Fundação Carlos Chagas Filho de Amparo à Pesquisa do Estado do Rio de Janeiro (FAPERJ) - Brasil.

Data availability

No data was used for the research described in the article.

References

Adams, M.L., Larsen, E.W., Pomraning, G.C., 1989. Benchmark results for particle transport in a binary Markov statistical medium. J. Quant. Spectrosc. Radiat. Transfer 42 (4), 253–266. http://dx.doi.org/10.1016/0022-4073(89)90072-1.

Alvim, A.C.M., 2007. Métodos Numéricos em Engenharia Nuclear. Ed. Certa, Paraná, Brazil.

Anon, 2008. Taylor expansions and applications. In: Mathematical Analysis I. Springer, pp. 223–255. http://dx.doi.org/10.1007/978-88-470-0876-2_7,

Barros, R.C., Filho, H.A., Valero Orellana, E.T., da Silva, F.C., do Couto, N., Dominguez, D.S., Hernández, C.R.G., 2003. The application of spectral nodal methods to discrete ordinates and diffusion problems in cartesian geometry for neutron multiplying systems. Prog. Nucl. Energy 42 (4), 385–426. http://dx.doi.org/10.1016/S0149-1970(03)90012-6.

Bitterli, B., Ravichandran, S., Muller, T., Wrenninge, M., Novak, J., Marschner, S., Jarosz, W., 2018. A radiative transfer framework for non-exponential media. In: SIGGRAPH Asia 2018 Technical Papers. New York, NY.

Booth, T.E., 2006. Power iteration method for the several largest eigenvalues and eigenfunctions. Nucl. Sci. Eng. 154 (1), 48–62. http://dx.doi.org/10.13182/NSE05-05.

da Silva, O.P., Guida, M.R., Filho, H.A., Barros, R.C., 2020. A response matrix spectral nodal method for energy multigroup x,y-geometry discrete ordinates problems in non-multiplying media. Prog. Nucl. Energy 125, 103288. http://dx.doi.org/10.1016/j.pnucene.2020.103288.

Davis, A.B., 2004. Effective propagation kernels in structured media with broad spatial correlations, illustration with large-scale transporte of solar photons through cloudy atmospheres. Comput. Methods Transp. Springer, New York.

Davis, A.B., Marshak, A., 2004. Photon propagation in heterogeneous optical media with spatial correlations: Enhanced mean-free paths and wider-than-exponential free-path distributions. J. Quant. Spectrosc. Radiat. Transfer 84 (3).

Davis, A.B., Mineev-Weinstein, 2009. Radiation transport through random media represented as measurable functions: Positive versus negative spatial correlations. In: International Conference on Advances in Mathematics, Computational Methods, and Reactor Physics. Saratoga, United States of America.

Davis, A.B., Xu, F., 2014. A generalized linear transport model for spatially correlated stochastic media. J. Comput. Theor. Transp. 43, 474–514.

de Abreu, M.P., Filho, H.A., de Barros, R.C., 1996. A numerical method for multigroup slab-geometry eigenvalue problems in transport theory with no spatial truncation error. Transport Theory Statist. Phys. URL https://www.tandfonline.com/doi/abs/10.1080/00411459608204830.

Dumas, L., Golse, F., 2000. Homogenization of transport equations on JSTOR. SIAM J. Appl. Math. 60 (4), 1447–1470, URL https://www.jstor.org/stable/118558.

Gandini, A., Salvatores, M., 2002. The physics of subcritical multiplying systems. J. Nucl. Sci. Technol. 39 (6), 673–686. http://dx.doi.org/10.1080/18811248.2002.9715249.

Ge, J., Wang, C., Xiao, Y., Tian, W., Qiu, S., Su, G.H., Zhang, D., Wu, Y., 2016. Thermal-hydraulic analysis of a fluoride-salt-cooled pebble-bed reactor with CFD methodology. Prog. Nucl. Energy 91, 83–96. http://dx.doi.org/10.1016/j.pnucene.2016.01.011.

Golderg, K., Newman, M., Haynsworth, E., 1964. Combinatorial analysis. In: Abramowitz, M., Stegun, I.A. (Eds.), Handbook of Mathematical Functions with Formulas, Graphs, and Mathematical Tables. Tenth Priting.

Gougar, H.D., Ougouag, A.M., Terry, W.K., Ivanov, K.N., 2010. Automated design and optimization of pebble-bed reactor cores. Nucl. Sci. Eng. 165 (3), 245–269. http://dx.doi.org/10.13182/NSE08-89.

Jarabo, A., Aliaga, C., Gutierrez, D., 2018. A radiative transfer framework for spatially correlated materials. ACM Trans. Graph. 37 (4), 83:1–83:13.

Kadak, A.C., 2005. A future for nuclear energy: pebble bed reactors. Int. J. Crit. Infrastruct. URL https://www.inderscienceonline.com/doi/abs/10.1504/IJCIS.2005.006679.

Larsen, E.W., 2007. A generalized boltzmann equation for non-classical particle transport. In: Proceedings of the International Conference on Mathematics and Computation and Supercomputing in Nuclear Applications. M&C + SNA, Monterrey, CA.

Larsen, E., Vasques, R., Vilhena, M., 2005. Particle transport in the 1-D diffusive atomic mix limit. In: Proceedings of International Topical Meeting on Mathematics and Computation, Supercomputing, Reactor Physics and Nuclear and Biological Applications. Avignon, France.

Larsen, E.W., Vasques, R., 2011. A generalized linear Boltzmann equation for non-classical particle transport. J. Quant. Spectrosc. Radiat. Transfer 112 (4), 619–631. http://dx.doi.org/10.1016/j.jqsrt.2010.07.003.

Lewis, E.E., Miller, W.F., 1993. Computational Methods of Neutron Transport. Wiley-Interscience, Illinois, USA.

Li-Po, L., Yi-Bao, L., Juan, W., Bo, Y., Tao, Z., 2008. The influence of reactor core parameters on effective breeding coefficient keff. Chin. Phys. B 17 (3), 896. http://dx.doi.org/10.1088/1674-1056/17/3/026.

Lohnert, G.H., Reutler, H., 1983. The modular HTR - a new design of high-temperature pebble-bed reactor. Nucl. Energy 22 (3), 197–200, URL https://inis.iaea.org/search/search.aspx?orig_q=RN:15031339.

Menezes, W.A., Alves Filho, H., Barros, R.C., Moraes, C.S., Dominguez, D.S., 2013. Analytical spatial reconstruction scheme for the coarse-mesh solutions generated by the constant spectral nodal method for monoenergetic discrete ordinates transport calculations in X,Y geometry fission–chain reacting systems. Ann. Nucl. Energy 53, 274–279. http://dx.doi.org/10.1016/j.anucene.2012.08.029.

Moormann, R., 2009. A safety re-evaluation of the AVR pebble bed reactor operation and its consequences for future HTR concepts. ASME Digit. Collect. 265–274. http://dx.doi.org/10.1115/HTR2008-58336.

Moraes, L.R.C., Alves Filho, H., Barros, R.C., 2020a. Estimation of neutron sources driving prescribed power generations in subcritical systems using one-speed two-dimensional discrete ordinates formulations. Ann. Nucl. Energy 136, 107053. http://dx.doi.org/10.1016/j.anucene.2019.107053.

Moraes, L.R.C., Barichello, L.B., Barros, R.C., Vasques, R., 2022a. On the application of the analytical discrete ordinates method to the solution of nonclassical transport problems in slab geometry. J. Comput. Phys. 455, 110982. http://dx.doi.org/10.1016/j.jcp.2022.110982.

Moraes, L.R., Barros, R.C., Filho, H.A., 2020b. Determinação de Fontes de Neutrôns que Conduzem Sistemas Subcríticos a Distribuições Prescritas de Potência. Trends Comput. Appl. Math. 21 (3), 425. http://dx.doi.org/10.5540/tema.2020.021.03.425.

Moraes, L.R.C., Barros, R.C., Vasques, R., 2023a. On a response matrix solver for slab-geometry neutral particle transport problems in the discrete ordinates and energy multigroup formulations considering non-uniform interior sources. J. Comput. Theor. Transp. 52 (1), 55–77. http://dx.doi.org/10.1080/23324309.2023.2194294.

Moraes, L.R.C., Filho, H.A., Barros, R.C., 2022b. On the calculation of neutron sources generating steady prescribed power distributions in subcritical systems using multigroup x,y-geometry discrete ordinates models. Ann. Nucl. Energy 168, 108854. http://dx.doi.org/10.1016/j.anucene.2021.108854.

Moraes, L.R.d.C., Mansur, R.S., Moura, C.A., Curbelo, J.P., Filho, H.A., Barros, R.C., 2021. A response matrix method for slab-geometry discrete ordinates adjoint calculations in energy-dependent neutral particle transport. J. Comput. Theor. Transp. 50 (3), 159–179. http://dx.doi.org/10.1080/23324309.2021.1914661.

Moraes, L.R.C., Patel, J.K., Barros, R.C., Vasques, R., 2022c. An improved spectral approach for solving the nonclassical neutral particle transport equation. J. Quant. Spectrosc. Radiat. Transfer 290, 108282. http://dx.doi.org/10.1016/j.jqsrt.2022.108282.

Moraes, L.R.C., Vasques, R., Barros, R.C., 2023b. On the occurrence of linearly dependent eigenvectors in nonclassical transport calculations. J. Quant. Spectrosc. Radiat. Transfer 295, 108407. http://dx.doi.org/10.1016/j.jqsrt.2022.108407.

Olson, G.L., 2007. Gray radiation transport in multi-dimensional stochastic binary media with material temperature coupling. J. Quant. Spectrosc. Radiat. Transfer 104 (1), 86–98. http://dx.doi.org/10.1016/j.jqsrt.2006.08.013.

Patel, J.K., Moraes, L.R.C., Vasques, R., Barros, R.C., 2022. Transport synthetic acceleration for the solution of the one-speed nonclassical spectral SN equations in slab geometry. J. Comput. Appl. Math. 401, 113768. http://dx.doi.org/10.1016/j.cam.2021.113768.

Pomraning, G.C., 1991. Linear Kinetic Theory and Particle Transport in Stochastic Mixtures | Series on Advances in Mathematics for Applied Sciences. 7, World Scientific Publishing Company, Singapore, http://dx.doi.org/10.1142/1549.

Pomraning, G.C., 2002. Transport theory in discrete stochastic mixtures. In: Advances in Nuclear Science and Technology. Springer, Boston, MA, USA, pp. 47–93. http://dx.doi.org/10.1007/0-306-47811-0_2,

Prinja, A.K., Larsen, E.W., 2010. General principles of neutron transport. In: Handbook of Nuclear Engineering. Springer, Boston, MA, USA, pp. 427–542. http://dx.doi.org/10.1007/978-0-387-98149-9_5,

Romojaro, P., Álvarez-Velarde, F., Kodeli, I., Stankovskiy, A., Díez, C.J., Cabellos, O., García-Herranz, N., Heyse, J., Schillebeeckx, P., Van den Eynde, G., Žerovnik, G., 2017. Nuclear data sensitivity and uncertainty analysis of effective neutron multiplication factor in various MYRRHA core configurations. Ann. Nucl. Energy 101, 330–338. http://dx.doi.org/10.1016/j.anucene.2016.11.027.

Stewart, J., 2009. Multivariable Calculus: Concepts and Contexts (Available 2010 Titles Enhanced Web Assign). Cengage Learning, Boston, MA, USA.

Su, B., Pomraning, G.C., 1993. Benchmark results for particle transport in binary non-markovian mixtures. J. Quant. Spectrosc. Radiat. Transfer 50 (2), 211–226. http://dx.doi.org/10.1016/0022-4073(93)90119-3.

Torquato, S., Truskett, T.M., Debenedetti, P.G., 2000. Is random close packing of spheres well defined? Phys. Rev. Lett. 84 (10), 2064–2067. http://dx.doi.org/10.1103/PhysRevLett.84.2064.

Vasques, R., 2013. Estimating anisotropic diffusion of neutrons near the boundary of a pebble bed random system. In: Proceedings of the International Conference on Mathematics and Computational Methods Applied To Nuclear Science & Engineering. Sun Valley, ID.

Vasques, R., Krycki, K., Slaybaugh, R.N., 2017. Nonclassical particle transport in one-dimensional random periodic media. Nucl. Sci. Eng. 185 (1), 78–106.

Vasques, R., Larsen, E.W., 2009. Anisotropic diffusion in model 2-D pebble-bed reactor cores. In: Proceedings of the International Conference on Advances in Mathematics. Saratoga Springs, NY.

Vasques, R., Larsen, E.W., 2014a. Non-classical particle transport with angular-dependent path-length distributions. I: Theory. Ann. Nucl. Energy 70, 292–300. http://dx.doi.org/10.1016/j.anucene.2013.12.021.

Vasques, R., Larsen, E.W., 2014c. Non-classical particle transport with angular-dependent pathlength distributions. II: application to pebble bed reactor cores. Ann. Nucl. Energy 70, 301–311.

Vasques, R., Moraes, L.R.C., Barros, R.C., Slaybaugh, R.N., 2020. A spectral approach for solving the nonclassical transport equation. J. Comput. Phys. 402, 109078. http://dx.doi.org/10.1016/j.jcp.2019.109078.

Wrenninge, M., Villemin, R., Hery, C., 2017. Path Traced Subsurface Scattering using Anisotropic Phase Functions and Non-Exponential Free Flights. Technical Memo 17-07, Pixar Inc..

Yang, X.-S., 2017. Chapter 3 - binomial theorem and expansions. In: Engineering Mathematics with Examples and Applications. Academic Press, Cambridge, MA, USA, pp. 31–35. http://dx.doi.org/10.1016/B978-0-12-809730-4.00004-5,